

# Neural Agonist–Antagonist Coupling in the Absence of Mechanical Coupling after Targeted Muscle Reinnervation

Laura Ferrante<sup>1\*</sup>, Anna Boesendorfer<sup>2</sup>, Benedikt Baumgartner<sup>2</sup>,  
Manuel Catalano<sup>4</sup>, Antonio Bicchi<sup>4,5†</sup>, Oskar Aszmann<sup>2,3†</sup>,  
Dario Farina<sup>1\*†</sup>

<sup>1</sup>Department of Bioengineering, Imperial College London, London, United Kingdom.

<sup>3</sup>Department of Plastic, Reconstructive and Aesthetic Surgery, Medical University of Vienna, Vienna, Austria.

<sup>2</sup>Clinical Laboratory for Bionic Extremity Reconstruction, Department of Plastic, Reconstructive and Aesthetic Surgery, Medical University of Vienna, Vienna, Austria.

<sup>4</sup>SoftRobotics Lab for Human Cooperation and Rehabilitation, Istituto Italiano di Tecnologia, Genoa, Italy.

<sup>5</sup>Research Center E.Piaggio, University of Pisa, Pisa, Italy.

\*Corresponding author(s). E-mail(s): [l.ferrante@imperial.ac.uk](mailto:l.ferrante@imperial.ac.uk);  
[d.farina@imperial.ac.uk](mailto:d.farina@imperial.ac.uk);

Contributing authors: [anna.boesendorfer@meduniwien.ac.at](mailto:anna.boesendorfer@meduniwien.ac.at);  
[benedikt.baumgartner@meduniwien.ac.at](mailto:benedikt.baumgartner@meduniwien.ac.at); [manuel.catalano@iit.it](mailto:manuel.catalano@iit.it);  
[antonio.bicchi@unipi.it](mailto:antonio.bicchi@unipi.it); [oskar.aszmann@meduniwien.ac.at](mailto:oskar.aszmann@meduniwien.ac.at);

†Equal contribution for senior authorship

## Abstract

Following limb amputation and targeted muscle reinnervation (TMR), nerves supplying agonist and antagonist muscles are rerouted into separate targeted muscles, disrupting natural neuromechanical coupling between muscle groups. Using high-density intramuscular microelectrode arrays in reinnervated muscles, we show that neural signals for agonist and antagonist tasks remain functionally coupled: motor units active during agonist tasks were also recruited during

corresponding antagonist tasks, despite no visual feedback on coactivation being provided.

**Keywords:** Targeted Muscle Reinnervation, motor units, common synaptic input, intramuscular electrodes, antagonist, synergy

## 1 Main

Limb amputation causes sensorimotor impairment, as both afferent and efferent neural pathways are irreversibly disrupted. Advanced nerve transfer techniques, such as Targeted Muscle Reinnervation (TMR) [Kuiken et al. \(2004\)](#) and Regenerative Peripheral Nerve Interfaces (RPNI) [Kung et al. \(2014\)](#), reduce neuroma-related phantom limb pain and support prosthetic-based sensorimotor rehabilitation. However, these procedures do not restore the neuromechanical coupling between agonist and antagonist muscles present in intact biological limbs.

In TMR, polyfascicular nerves that once innervated multiple muscles and supported distinct functions (i.e., polyvalent nerve) of the limb are redirected into a single targeted muscle. Importantly, nerves carrying agonist and antagonist signals are rerouted into biomechanically uncoupled targeted muscles (Fig.1-a,d,c,d). In RPNI, nerves are surgically split into fascicles, each rerouted into a separate muscle graft.

This nerve–muscle reorganisation disrupts mechanical interactions between antagonistic and synergistic muscles, impairing afferent signalling from spindles and Golgi organs [Proske and Gandevia \(2012\)](#) and consequently disrupting neural processes at the base of limb proprioception and motor coordination. Although spindles reinnervation occurs in animal models of TMR [Festin et al. \(2024\)](#), its extent and functional role in humans remain unclear. Consequently, residual muscle contraction in amputees is often inconsistent and prone to unintended coactivation [Seyedali et al. \(2012\)](#); [Huang and Huang \(2018\)](#); [Zuniga et al. \(2018\)](#), complicating the control of bionic limbs.

In TMR patients, electromyographic (EMG) signals recorded with bipolar surface electrodes from separate reinnervated muscles are used to control these opposing functions on prosthetic limbs [Kuiken et al. \(2004\)](#). However, since reinnervated muscles receive input from polyfascicular nerves, bipolar surface EMG signals likely reflect a mixture of neural commands, making it unclear whether these signals reflect distinct functional roles such as agonist–antagonist specificity.

Here, we study the neural signals underlying co-activation in muscles reinnervated by polyfascicular nerves that once innervated agonist-antagonist muscle groups of the upper limb in TMR patients, in the absence of any feedback on such co-activation. We hypothesized that the central nervous system continues to coordinate agonist and antagonist muscle commands. This would occur even when the neural signals controlling opposing actions arise from the same nerve, and are therefore displayed by the same targeted muscle as a result of polyfunctional reinnervation. For example, the extensor carpi radialis brevis and the extensor carpi ulnaris are both supplied by the radial nerve and act as synergists for wrist extension, yet they behave as antagonists

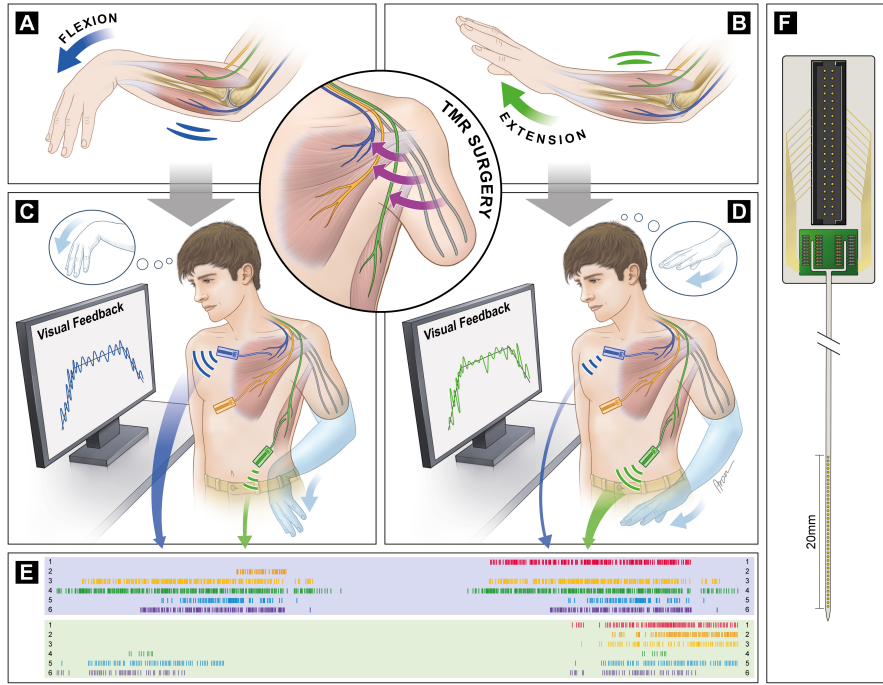


**Fig. 1 Micro-electrode arrays record residual neural coupling in muscles reinnervated by transferred polyfascicular nerves during agonist and antagonist tasks.** **a-b**, In persons with intact upper limbs, the neural control of movement, e.g., wrist flexion and extension, involves the activation of groups of agonist and antagonist muscles spanning relevant articular joints. **c-d**, Loss of peripheral tissue after amputation leads to a disruption of the neuro-mechanical coupling between agonist and antagonist muscles of the upper limb. A transhumeral patient had the residual ulnar (blue), median (orange) and radial (green) nerves transferred to targeted muscles via Targeted Muscle Reinnervation (TMR) surgery. The participant was asked to perform agonist-antagonist tasks with his missing limb (e.g., wrist flexion and extension) while the intramuscular activity of all reinnervated muscles was recorded using micro-electrode arrays (panel **f**) inserted percutaneously into the muscles. The median across-channel EMG activity of the reinnervated muscle defined as the agonist for a given task (e.g., the upper portion of the pectoralis major reinnervated by the ulnar nerve for wrist flexion), was displayed on a screen as real-time visual feedback. In panels **c** and **d**, the participant performed different tasks and thus received visual feedback from different micro-electrode arrays. The participant had to match a target trapezoidal activation profile with his muscle activity. **e**, In an offline analysis, for each task, we decomposed the neural signals recorded by the "agonist" and "antagonist" micro-electrode arrays (blue and green) into constituent motor unit spike trains by blind-source separation. Corresponding motor unit spike trains are shown in the top (shaded blue) and bottom (shaded green) figure, during wrist flexion and extension. Tracking of motor units across the two tasks revealed that during wrist flexion, the micro-electrode array recording the activity of the "antagonist" muscle detected motor units that were functionally relevant and matched some of those recruited when the subject performed the corresponding antagonist task, i.e., wrist extension. For example, all 3 motor units detected by the "antagonist" (green) micro-electrode array during wrist flexion were recruited during wrist extension, when the TMR muscle had an antagonist role. **f**, Schematic of high-density micro-electrode array Muceli et al. (2022) consisting of 40 channels (diameter of 140 µm) linearly distributed over a length of 2 cm with inter-electrode distance of 500 µm. Note that in panels **A** and **B**, a representative agonist and antagonist muscle pair is shown for simplicity. The neural structures and micro-electrode array are not represented with accurate scaling to improve clarity.

during hand abduction–adduction. We further posited that such coordination would persist when commands were distributed across biomechanically separated muscles, supplied by different polyfascicular nerves.

This hypothesis was investigated in three TMR patients (P1, P2, P3). Patient P3 (aged 53, glenohumeral amputation) previously participated in our study [Ferrante et al. \(2025\)](#) where we demonstrated a biological interface that combines polyfascicular TMR with high-resolution intramuscular microelectrode recordings to isolate task-specific neural signals of the missing limb.

We reanalyzed data from patient P3, who had microelectrode arrays implanted in the pectoralis minor (P3-TMR1) and latissimus dorsi (P3-TMR2), reinnervated by the ulnar and radial nerves, respectively. Since only two agonist–antagonist task pairs were recorded for P3, two additional participants were recruited (P1 and P2; aged X and 63, transhumeral amputation). In P1, the median and ulnar nerves were rerouted to the anterior deltoid (P1-TMR1) and the radial nerve to the posterior deltoid (P1-TMR2). In P2, the ulnar, median, and radial nerves were transferred to the pectoralis minor (P2-TMR1), abdominal pectoralis major (P2-TMR2), and latissimus dorsi (P2-TMR3), respectively (Fig. 1). Participants' details are provided in Tab. 1 (Online Methods). In this work, given a movement of the missing limb, we identified the primary agonist and antagonist reinnervated muscles based on the original function of their rerouted nerves. In Fig. 1-c,d, P2's TMR1 and TMR3 muscles, reinnervated by the ulnar (blue) and radial (green) nerves, were considered as agonists for wrist flexion and extension, respectively, and as antagonists for the opposite movement. The experimental paradigm was designed such that subjects received visual feedback only from the agonist muscle, preventing voluntary modulation of antagonist activity, while intramuscular signals were recorded from both muscles (Fig. 1-c,d). This enabled assessment of intrinsic coactivation patterns, providing insight into the extent to which neural coupling between agonist and antagonist pathways was preserved and functionally expressed. Building on previous findings [Ferrante et al. \(2025\)](#), we used a 40-channel high-density micro-electrode array [Muceli et al. \(2010\)](#) (Fig. 1-f) to record the activity of agonist–antagonist reinnervated muscle of P1 and P2 as participants performed three and eight pairs of agonist–antagonist tasks, respectively. We re-used data about two pairs of tasks for P3. In total, six, sixteen and four tasks of the missing limb were recorded from three participants, respectively. Channels with baseline noise  $> 15 \mu\text{V}$  were removed. Intramuscular EMG was decomposed into motor unit spike trains via blind source separation [Muceli et al. \(2022\)](#) and refined using EMGLAB [McGill et al. \(2005\)](#). Motor units with sparse firings or low pulse-to-noise ratio were discarded (Online Methodology, Section 3.5).

Across all tasks, 15, 78, and 19 motor units were reliably decomposed from agonist reinnervated muscles in P1, P2, and P3 (average number:  $2.5 \pm 1.2\%$ ,  $4.9 \pm 2.4\%$ ,  $4.5 \pm 2.4\%$ ), and 11, 61, 12 motor units were decomposed from corresponding antagonist reinnervated muscles (average number:  $1.8 \pm 1.6\%$ ,  $3.8 \pm 1.5\%$ ,  $3.5 \pm 0.6\%$ ). Importantly, since visual feedback was provided only for the agonist muscles, motor units recorded from the antagonist muscles reflected natural coactivation patterns.

Motor units were tracked across tasks to identify if they were unique or shared. In particular, for each reinnervated muscle, motor units were tracked to determine

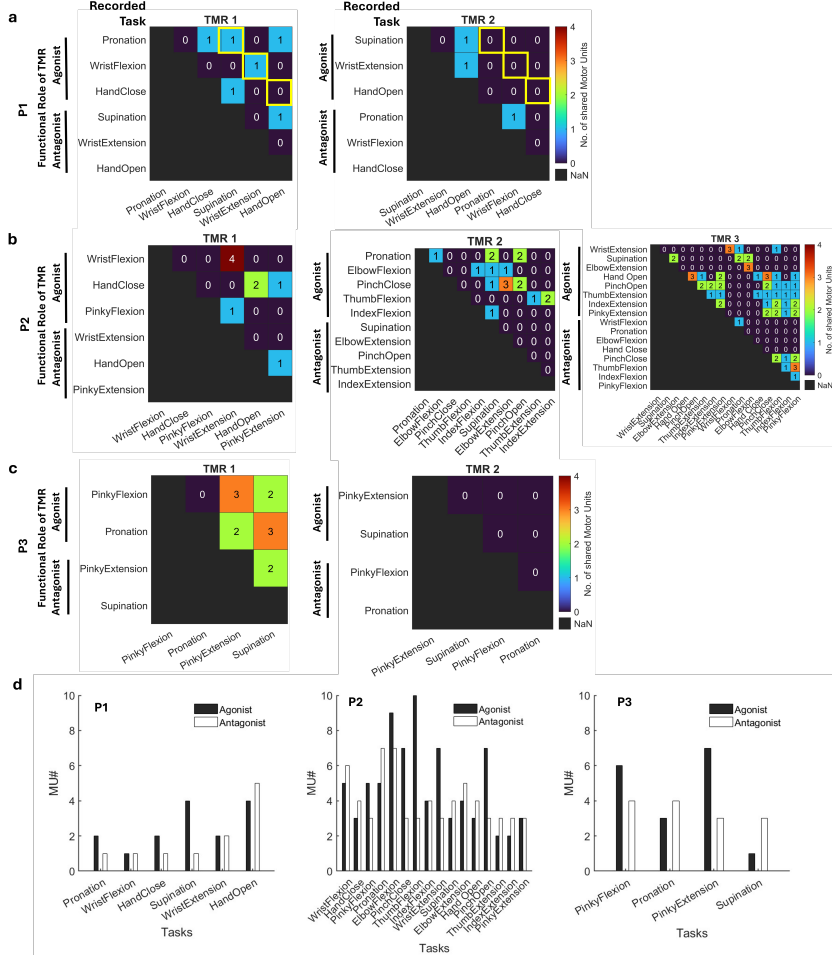


**Fig. 2 a,b,c.** For each patient (P1, P2, P3) and reinnervated muscle (TMRX), the diagrams detail the relation between recorded tasks in terms of the number of shared motor units. Given a task (“recorded task”), a TMR muscle may have an agonist/antagonist role depending on its rerouted nerve. For each task, an agonist and an antagonist TMR muscles were identified, and the intramuscular signals were recorded. E.g., when P2 performed wrist flexion, TMR1 provided agonist signals and thus this task is labelled as “agonist”. TMR3 of P2 provided agonist neural signals for wrist extension. Wrist extension task was thus labelled as agonist in TMR3, but as antagonist in TMR1. The diagrams show the relationship between “agonist” motor units and motor units recruited when the antagonist task was performed (squares highlighted in yellow). It can be observed that some of the motor units recruited during agonist tasks were also active during the corresponding antagonist task (e.g., the same TMR muscle had an agonist and antagonist role). **d.** Total number of motor units identified per movement when this had an agonist or antagonist role. E.g., two and one MUs were recruited by P1 during Pronation (agonist function) and Pronation (antagonist function, i.e., recorded during wrist supination).

if those recruited as agonists were also active when the same muscle acted as an antagonist. For example (Fig. 1-E), six motor units were decomposed from recordings in TMR1 during wrist flexion (on the left, shaded blue), with four of these also active

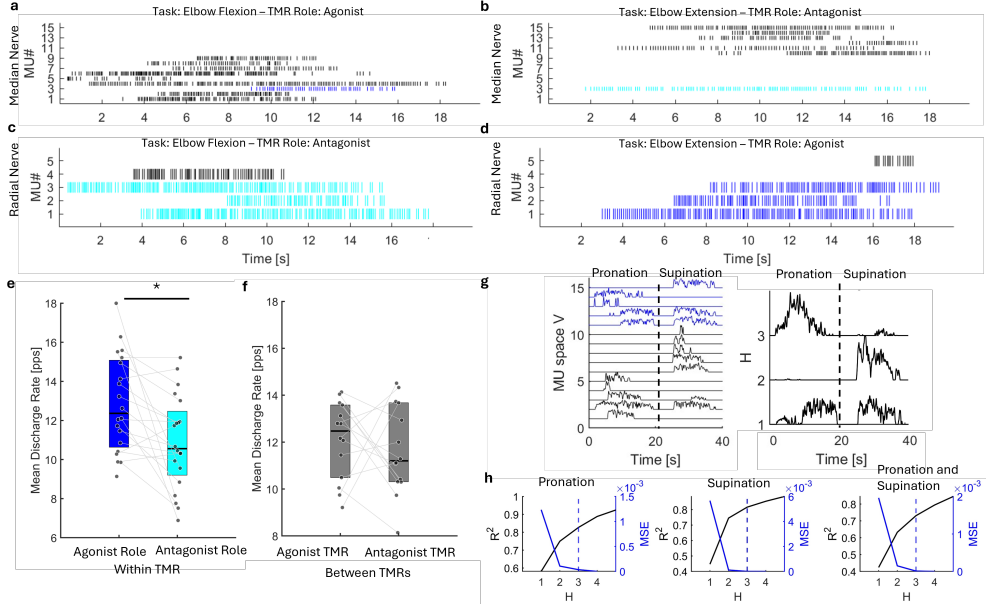


**Fig. 3 Discharge properties of motor units in reinnervated muscles with agonist and antagonist roles for a given task and neural manifold analysis.** In panels a-d, we show the spike trains of motor units reliably decomposed using a micro-electrode array into the targeted muscle reinnervated by the median nerve (a-b) and radial nerve (c-d). These nerves carry neural signals for elbow flexion and extension tasks, respectively. Hence, during elbow flexion, "agonist" motor units are displayed in panel (a), whereas antagonist ones are shown in panel (c). Viceversa, during elbow extension, the radial nerve carries "agonist" signals (d) and the median nerve antagonist ones (b). For each reinnervated muscle, we tracked and colour-coded motor units active during both elbow flexion and extension tasks. In panel a, motor unit 4 (blue) is also active during elbow extension (light blue in panel b). Similarly, motor units 1-3, which have an agonist role for elbow extension (d, blue), are recruited during elbow flexion (panel c, light blue). e, we computed the mean discharge rate of each motor unit active in both a and b or c and d, as the mean of the inverse of inter-spike-intervals during the plateau phase of the contraction in the "agonist" reinnervated muscle. The discharge rate of motor units in the "antagonist" reinnervated muscle is computed within the same time window. We assessed whether motor units had a different mean discharge rate during corresponding agonist and antagonist tasks. The distribution of mean discharge rates of motor units with an agonist role (color coded in blue as in panels a and d) is displayed in the "Agonist Role" group, while antagonist motor units (light blue in panel b and c) are shown in the "antagonist role" group. Each group contains 18 points (motor units across all tasks). The two-sided Wilcoxon signed-rank test is used to assess statistically significant differences between the two groups (p-value < 0.005). Statistical significance is indicated with a bar and asterisk. f, For each task, we consider the average mean discharge rate of motor units recorded in the agonist and correspondent antagonist reinnervated muscle. All detected motor units are used, e.g., the average mean firing rate of motor units in panel a and motor units in panel c constitute a pair of values in "Agonist TMR" and "Antagonist TMR". g, Neural manifold analysis for exemplary task for P2. On the left, a 15-dimensional MU space (V) is obtained by concatenating smoothed discharge rates of motor units recruited during pronation and supination in TMR1 (black) and TMR2 (blue). The dimensionality of the latent space (H) embedded in V is estimated using Non-Negative matrix Factorization (NNMF). The time-varying latent signals are shown on the left for the estimated dimensionality equal to 3. h, R<sup>2</sup>-curve obtained by applying NNMF on V with increasing latent space dimensionality (from 1 to 5). A dimensionality of 3 (dashed line) was estimated when considering MUs recruited during pronation, and supination only, as well as when considering the concatenated data (See Methodology for details).

during wrist extension when TMR1 acted as an antagonist (on the right, shaded blue). In P1, 40% of TMR1 motor units were shared between agonist and corresponding antagonist tasks, with none in TMR2. In P3, 60% and 0% were shared for TMR1 and TMR2. On average, across P2's three reinnervated muscles,  $42.3 \pm 24.7\%$  of agonist motor units were also recruited when the same muscle acted as antagonist. Figure 2 (highlighted in yellow) shows the number of motor units recruited during both agonist and corresponding antagonist tasks. In all participants, some units were also shared across other tasks of the missing limb, reflecting a degree of synergistic activity.

P1 and P3 are excluded from the remaining analysis due to the limited number of recorded tasks and decomposed motor units. In particular P1, had more difficulty in imagining and executing the tasks of his missing limb.

For each task performed by P2, we compared firing rates of motor units of the same reinnervated muscle when acting as agonist versus antagonist (e.g., units 3–6 in Fig. 1-E during wrist flexion vs. extension) to test if they were similar (null hypothesis). A significant difference ( $p = 0.002$ , two-sided Wilcoxon signed rank test) was found between the distribution of average firing rate (MFR) of motor units (Fig. 3-e) when these had an agonist (blue, Fig. 3-a,d) or antagonist role (light blue, Fig. 3-b,c). When individual tasks were examined, no significant differences were found in MFR ( $p = 0.28$ , Fig. 3-f) between motor units of agonist and antagonist reinnervated muscles (e.g., Fig. 3-a,c). No significant differences were found in recruitment threshold or coefficient of variation. See Methodology for metrics details.

In individuals with intact limbs, agonist–antagonist coordination involves supraspinal and spinal mechanisms and emerges from the projection of common and independent synaptic inputs to relevant motor neuron populations and the integration of afferent inputs. Common input is reflected in shared low-frequency oscillations in motor neuron discharge. We assess the dimensionality of common input to motor units recruited for agonist–antagonist tasks by estimating the neural manifold underlying neural signals of recruited motor units. For each pair of agonist–antagonist tasks, spike trains of recruited motor units were tracked, combined, and smoothed with a 0.4s Hanning window. The total number of unique motor units defined the dimensionality of the motor unit space  $V$  (Fig. 3-g, left). Non-Negative Matrix Factorization [Lee and Seung \(2000\)](#) was used to estimate the neural manifold  $H$  (Fig. 3-g, right side), with dimensionality estimated according to [Clark et al. \(2010\)](#) (Fig. 3-h). We hypothesized a minimum dimensionality of two, reflecting two distinct sources of common input to motor units recruited for agonist and antagonist tasks. While task complexity and non-synchronous motor neural activity may contribute to increasing the manifold dimensionality, this was at least two for each pair of tasks, indicating that agonist and antagonist motor units were not dominated by co-activation despite TMR and altered afferent pathways. Analysis of individual tasks (without concatenating motor units of agonist and antagonist tasks) confirmed a manifold dimensionality greater than one.

The functional relationship between agonist and antagonist muscles is shaped by continuous sensory integration, efferent commands, task constraints, and limb–environment interactions. Under stable conditions, reciprocal inhibition via

afferent pathways facilitates agonists contraction by inhibiting motor units of the antagonist muscles [Pierrot-Deseilligny and Burke \(2005\)](#). However, agonist–antagonist coactivation is commonly observed under time or accuracy constraints [Poscente et al. \(2021\)](#); [Danion and Galléa \(2004\)](#) or task uncertainty [Burdet et al. \(2001\)](#); [Franklin et al. \(2003\)](#). In these cases tonic muscle coactivation is thought to overcome spinal reciprocal inhibition, potentially facilitating antagonist muscle activity.

Although this study cannot determine whether the observed coactivation reflects a voluntary strategy or results from altered excitation–inhibition balance in the neural circuit, we found that agonist–antagonist co-activation persisted after TMR. The functional specificity of this neural activity indicates the presence of residual neural coupling between agonist and antagonist pathways, likely mediated by intact spinal and supraspinal mechanisms not affected by amputation and TMR. Such persistent functional neural coupling may be exploited for controlling advanced prostheses with variable stiffness actuators, allowing amputees to modulate the dynamics of movement besides the kinematics, and for artificial substitution of sensory feedback associated with joint impedance and movement perception.

## 2 Methods/Online content

### 2.1 Participant

Three participants (all male; 62, 65, 53 years old) were recruited for this study. The study was approved by Ethics Committee of Imperial College (reference number: 19IC5641) and performed according to the Declaration of Helsinki. Before the experimental session, the participant provided written informed consent. P1 suffered an accident in 1994 which included a plexus injury and resulted in a left transhumeral amputation. 20 years after the accident, TMR surgery was performed, resulting in muscle signals in his deltoid muscle, now being mediated by the ulnar and median nerves in the anterior part and by the radial nerve in the posterior part of the muscle. He controlled his myoelectric prosthesis with the help of two bipolar surface electrodes. P2 had transhumeral amputation of his left upper limb and underwent TMR surgery by nerve-to-nerve coaptation ([Pettersen et al. \(2024\)](#)), mainly to treat phantom limb pain, 8 years before the current study. The ulnar nerve was transferred to the pectoralis minor muscle, the median nerve to the lower (abdominal) part of the pectoralis major muscle, and the radial nerve to the latissimus dorsi muscle. The pectoralis minor was released from the coracoid process and was transferred into the axilla to enable easier detection of the EMG signals. The participant daily uses a myoelectrical prosthesis, controlled with two standard surface bipolar electrodes positioned on the remaining (non-reinnervated) triceps and biceps muscles of the limb. 20 years before this study, P3 had his left arm amputated at the glenohumeral level and underwent TMR surgery 8 years after the amputation. After this procedure, he could use 6 surface bipolar electrodes in order to operate his myoelectric prosthesis.

TMR volunteers	P1	P2	P3
<b>Patient characteristics</b>			
Age	62 y	63 y	53 y
Time since amputation	28 y	45 y	20 y
Level of amputation	transhumeral	transhumeral	glenohumeral
<b>Surgery details</b>			
Time from TMR surgery	8 y	8 y	13 y
TMR site and innervating nerve	Anterior Deltoid, Ulnar + Median (TMR1) Posterior Deltoid, Radial (TMR2)	Pec. Major pars abdominalis, Median (TMR1) Pec. Minor, Ulnar (TMR2) Latissimus Dorsi, Radial (TMR3)	Pec. Major pars clavicularis, MC Pec. Minor, Ulnar (TMR1) Pec. Major pars sternocostalis, Median part I (lat.) Pec. Major pars abdominalis, Median part II (med.) Latissimus dorsi/ Teres major, Radial (TMR2)
<b>Prosthesis information</b>			
Prosthetic type	Myoelectric	Myoelectric	Myoelectric
Prosthetic use	16h/day	15h/day	0-12h/day for 1-2 days/week
No. of used EMG sensors	2	2	6
Movements for prosthetic control	fist and elbow extension	elbow flexion and extension	tripod, fingers extension, elbow extension-flexion, pronation-supination
Natural phantom limb position	30° elbow flexion, forearm neutral, hand slightly closed	20° elbow flexion, wrist neutral, 30° abduction, hand slightly open	90° elbow flexion, forearm neutral, hand closed (fist)

**Table 1** Patient characteristics, surgery details, prosthetic information and experimental protocol. h: hours; MCP: metacarpophalangeal joint; MVC: maximal voluntary contraction; P1: patient 1; P2: patient 2; P3: patient 3; reps: repetitions; s: seconds; TMR: targeted muscle reinnervation, y: years, (-): comment of patients that the movements were difficult to imagine for the patient; \* for these movements a different protocol (see \*) was applied.

## 2.2 Apparatus for electrophysiological recordings in targeted reinnervated muscles

The intramuscular electromyographic activity of each reinnervated muscle was measured using a micro-array described by Muceli *et al.* [Muceli et al. \(2022\)](#). The micro-array included 40 platinum channels (area of 5,357  $\mu\text{m}^2$ ) linearly distributed with an interelectrode distance of 500  $\mu\text{m}$  over 2 cm of a double-sided polyimide structure 20  $\mu\text{m}$  thick. For each reinnervated muscle, the most myoelectrically active part of the muscle was identified through clinical examination (palpation, visual muscle contraction by performing different missing limb movement tasks related to the nerve transferred into the reinnervated muscle) and surface EMG measurements with the MyoBoy (Ottobock Healthcare Products GmbH, Duderstadt, Germany) and used as the insertion point for the micro-array. After disinfecting the skin, the micro-arrays were inserted acutely into the muscle at a flat angle, using a hypodermic needle of a similar size to those used in conventional concentric needle recordings. The needle was then removed while ensuring the micro-array stood in place in the muscle. The entire insertion procedure was aided by using a portable ultrasound scanner. The micro-array was removed at the end of the experimental session, and the skin was disinfected. A detailed insertion procedure is reported in Section 1 of the Supplementary material. The EMG signals were recorded in monopolar configuration using a multichannel amplifier (Quattrocento, OT Bioelettronica, Torino, Italy) with a gain of 150 and band-pass-filtered (10-4,400 Hz) before being sampled at 10,240 Hz using an A/D converter to 16 bit. The reference and ground electrodes were placed in areas of no significant myoelectric activity on the stump. Each microarray provided 40 active recording channels.

### 2.3 Experimental protocol

The participant sat in front of a computer screen and received visual feedback on the EMG activity recorded by the micro-array in reinnervated muscle. The signal used as visual feedback was the bipolar signal derived from the micro-electrode array that resulted in maximum amplitude. The volunteer was requested to perform specific movements of their missing limb while contracting the reinnervated muscle. The list of missing limb movements/tasks to include in the protocol was planned to account for individual needs (e.g., ability to sustain longer contractions), and according to the nerve transfer matrix. At the beginning of each task, the MVC was recorded and used to normalize the EMG signals of the contractions for the particular task. The volunteer was then requested to contract the reinnervated muscle and modulate the EMG activity to accurately track a series of target trapezoidal trajectories displayed on the computer screen. Each trapezoidal trajectory consisted of (i) a positive ramp phase where the muscle contraction had to be increased up to a % of MVC; (ii) a constant contraction phase where the muscle contraction had to be maintained at a % of MVC; and finally (iii) a negative ramp down phase where the muscle contraction had to be decreased until the muscle was fully relaxed. For example, P1 had to (i) increase the muscle contraction from 0 to 10% of MVC in 4s; (ii) maintain the contraction level at 10% of MVC for 10s; and (iii) decrease the muscle contraction in 4s. The trapezoidal task was repeated 4 times per task. 20s of rest was allocated between each contraction to minimize fatigue.

### 2.4 Signal processing of EMG signals and quality assessment

The recorded intramuscular EMG signals were high-pass filtered at 1,000 Hz with a zero-lag first-order digital filter. The quality of the signals was assessed by computing the root-mean-square of 5s of data recorded at rest before starting the trials. Channels yielding a baseline noise  $> 15 \mu\text{V}$  were visually inspected and removed.

### 2.5 Motor unit decomposition

Each channel of the micro-array recorded an EMG signal given by the superimposition of the action potential propagating bidirectionally along the muscle fibers innervated by active motor neurons in the pick-up area of the electrode. Because fibers innervated by different motor neurons are intermingled, one channel might record the action potentials of multiple motor units. Moreover, the electrical activity of a motor units might be recorded by adjacent channels depending on the position of the electrode within the motor unit territory (i.e., the space defined by the fibers innervated by a motor neuron). Since each action potential is uniquely associated with a motor unit due to the high reliability of the neuromuscular junction [Wood and Slater \(2001\)](#), the motor unit spike events can be extracted by explaining multiple observations of the motor unit activity using multi-channel electrodes (observations). The problem of decomposition is thus formulated as a blind source separation problem.

The EMG signals were decomposed into their constituent motor unit spike trains using the algorithm described by Holobar and Zazula [Holobar and Zazula \(2007\)](#) and validated by Muceli *et al.* [Muceli et al. \(2022\)](#) using the same micro-arrays adopted in

this study. For each task, the decomposition of signals recorded by an electrode was inferred using all the data from the repetitions. The outcome of the automatic decomposition was validated by an expert investigator using EMGLAB [McGill et al. \(2005\)](#). Specifically, each EMG signal was inspected to detect decomposition errors such as missing or incorrectly assigned discharges, paying attention to instances of long or short interspike intervals. Detection of superimposition of motor unit potentials was aided by the multi-channel recordings; each channel of the micro-array may sample a different part of the motor unit territory, providing a unique observation of the motor unit electrical activity. While the action potential morphology (i.e., amplitude, shape) differs across channels, the firing pattern is the same. This redundant information is used to resolve superimpositions of action potentials from multiple motor units. When the spike train of a motor unit was fully identified, EMGLAB subtracted the template of the MUAPs from the EMG signals. When the power of residual signal was comparable to the baseline noise level the decomposition was considered completed. Small potentials and potentials resulting in bursts of activation were not decomposed for lack of accuracy. This procedure was repeated for each of the 40 channels of the electrode. To ensure that the same motor unit was being identified throughout the repetitions, we calculated the average MUAP per repetition by spike-triggered-averaging, i.e., by averaging the EMG signal of each channel on the intervals of 20 ms centred around the motor unit discharges obtained from decomposition of a repetition. We then computed the coefficient of determination  $\rho$  between the normalised MUAP templates and the ones of the other repetitions; additionally, motor units were the same across repetitions if their action potentials had maximum peak-to-peak amplitude on the same channel. Finally, we identified motor units that were satellite potentials of other units by computing the rate of agreement [Holobar et al. \(2010\)](#) between pairs of discharge patterns. The rate of agreement was defined as the ratio between the number of discharges that were present in both discharge patterns (common) and the sum of the number of common discharges and the number of discharges present in only one of the two discharge patterns. A tolerance of 10 samples ( $< 1$  ms) was used when identifying common discharges and accounting for propagation delays between the main potential and the satellite one. If the rate of agreement between two motor units exceeded 80% the motor unit with later discharges was considered a satellite potential of the first motor unit, removed from the motor unit list.

As a result of automatic and manual decomposition, the firing instances of the active motor units on each of the 40 channels were obtained.

## 2.6 Screening of motor units

Motor units with few sparse firings were removed. We consider only motor units whose spike trains were identified with a Pulse-to-Noise-Ratio  $\geq 30$  dB [Holobar et al. \(2014\)](#), a signal-to-interference metric introduced to quantify how accurately a motor unit signal can be distinguished given the background noise of the signal.

## 2.7 Firing properties of motor units

The following analysis was performed for each repetition of the different tasks. The histogram of the inter-spike intervals for each active motor unit was computed using 1-ms bins. Inter-spike intervals longer than 250 ms were considered as reflecting pauses in motor unit tonic activity and were removed from the inter-spike intervals of the motor unit. The distribution of the inter-spike intervals was tested for normality using the D'Agostino-Pearson's test ( $\alpha = 0.95$ ) [D'agostino et al. \(1990\)](#) before characterising the average firing rate of motor units. The median firing rate (MFR) was computed as the median of the inter-spike intervals of motor units since these had a non-normal distribution. The variability of the motor unit discharges was quantified using the CoV [%], computed as the ratio between the median and the standard deviation of ISIs. The smoothed firing rate for a motor unit was calculated by passing a Hanning window of 0.4 s over the impulse train corresponding to the firing times of that motor unit (instantaneous firing rate).

## 2.8 Motor unit tracking across tasks

Given the list of motor units decomposed for a task of a reinnervated muscle, we assess whether those units were recruited for other tasks of the same reinnervated muscle (i.e., motor units shared across tasks). For each pair of motor units of two tasks we calculated the (i) coefficient of determination between the normalised Motor Unit Action Potential (MUAPs) template obtained by spike-triggered averaging in a 20 ms window on the channel where the peak-to-peak unipolar amplitude of MUAPs was the largest; (ii) the distribution of the MUAP across channels was estimated as detailed above by concatenating the average MUAPs obtained for each channel to build an image of the spatial distribution of the MUAP potential (channels x time x motor unit amplitude). A 15% threshold was applied to the absolute amplitude of pixels and used to segment the area occupied by the MUAP. The MUAP cross-section (i.e., channels spanned by MUAP) was obtained by projecting the segmented area on the channel axis. Two MUAPs were flagged as belonging to the same motor units if  $\rho \geq 0.85$  or if their cross-section overlapped; visual inspection assessed the match between two motor units.

## 2.9 Task-dependent latent neural manifolds

For each reinnervated muscle (TMR*i*), the neural space embedded in the space defined by motor units decomposed for multiple tasks  $\mathbf{V}^i$  is estimated using NNMF. For each pair of agonist-antagonist, the matrix  $\mathbf{V}^i$ , of dimension  $m \times t$ , is obtained by (i) concatenating the smoothed spike trains of motor units active during agonist and corresponding antagonist task; (ii) by normalising the smoothed spike-trains to have unit variance. The variable  $m$  indicates the total number of independent motor units across agonist and antagonist task, hence smoothed spike trains of shared motor units are located in the same row of  $\mathbf{V}^i$ . According to NNMF,  $\mathbf{V}^i$  is mathematically described as follows:

$$\mathbf{V}^i \approx \mathbf{W}^i \mathbf{H}^i \quad (1)$$

where  $\mathbf{W}^i$  is the non-negative basis matrix  $\mathbf{V}^i$  of dimension  $m$  by  $l$ , and  $\mathbf{H}^i$  of dimension  $l$  by  $(r \times t)$  is the non-negative matrix of latent time-dependent variables. Each column of  $\mathbf{W}^i$  represents the contribution of the  $m$  motor units to the latent signals  $l$ . Each row of  $\mathbf{H}^i$  is a latent variable comprising the time-dependent input to motor units. NNMF solves a non-convex optimisation problem (i.e., minimises the reconstruction error defined as the Euclidean distance between  $\mathbf{V}^i$  and  $\mathbf{W}^i\mathbf{H}^i$ ), prone to converging to local minima. For this reason, given  $l$ , NNMF is repeated 10 times with random initialisation of  $\mathbf{W}^i$  and  $\mathbf{H}^i$  [Cheung et al. \(2009\)](#) and random shuffling of motor units spike trains in  $V_i$  and task repetitions concatenation order; the maximum number of iterations is set to 100. The latent space dimension  $l$  is set equal to the minimum number of latent factors explaining a significant portion of the total variance within  $\mathbf{V}^i$ . In our study, NNMF is applied for values of  $l$  ranging from 1 to 5. The coefficient of determination  $R^2$  is computed as in [Muceli et al. \(2010\)](#) [Muceli et al. \(2010\)](#). The MSE values are reported for completeness. The number of latent factors is determined using the  $R^2$ -curve as in [d'Avella et al. \(2003\)](#) [d'Avella et al. \(2003\)](#) and [Clark et al. \(2010\)](#) [Clark et al. \(2010\)](#).

## 2.10 Statistical analysis and reproducibility

Shapiro–Wilk tests were used to confirm homogeneity of variance and normal distribution of data respectively. Kruskal–Wallis one-way Anova analysis was undertaken since data violated parametric assumptions and used to analyse differences between reinnervated muscles for specific properties of motor units. The D'Agostino-Pearson's test was used to test the inter-spike intervals distribution for normality. Statistical significance was assumed at  $P \leq 0.05$ . All data is reported as mean  $\pm$  standard deviation.

The following steps were implemented to ensure reproducibility: (i) the analysis uses only motor units that could be accurately decomposed; (ii) We used an automatic EMG decomposition algorithm extensively validated on various datasets and manually assessed the results using the spike-sorting software EMGLAB to identify and correct decomposition errors; (iii) tracking of motor units was done automatically and visually inspected by an expert examiner to ensure correctness.

**Supplementary information.** If your article has accompanying supplementary file/s please state so here.

Authors reporting data from electrophoretic gels and blots should supply the full unprocessed scans for key as part of their Supplementary information. This may be requested by the editorial team/s if it is missing.

Please refer to Journal-level guidance for any specific requirements.

**Data availability.** The data supporting the findings are included in the article and Supplementary material. Raw data are available from the corresponding authors upon reasonable request. A sample of source data is provided with this paper.

**Code availability.** Available open source software was used for decomposition and manual editing. The code used for data analysis and figure generation is available from the corresponding authors upon reasonable request.

**Acknowledgments.** This work was supported by the European Research Council Synergy Grant Natural BionicS (810346). The authors thank Aron Cserveny (<https://www.sciencevisual.at/>) for conveying key concepts of the work through exceptional illustrations. We thank Aritra Kundu for helping with motor unit decomposition.

**Author contributions.** L.F., D.F., O.C.A., A.B. conceived this study, L.F., A.B., B.B. and O.A. performed the data acquisition, L.F. conducted the analysis, L.F. and D.F. interpreted the data, L.F. contributed to the first draft of the manuscript. All authors edited the manuscript for important scientific content and all approved the final version.

**Competing interests.** The authors declare no competing interests.

## Additional information

**Extended data.** Data supporting the findings of the article are included in the Article. A sample of intramuscular signals is made available. Additional data may be available from the corresponding authors upon reasonable request.

**Correspondence and request for materials.** should be addressed to L.F., D.F.

## Extended data

### References

Burdet E, Osu R, Franklin DW, et al (2001) The central nervous system stabilizes unstable dynamics by learning optimal impedance. *Nature* 414(6862):446–449

Cheung VC, Piron L, Agostini M, et al (2009) Stability of muscle synergies for voluntary actions after cortical stroke in humans. *Proceedings of the National Academy of Sciences* 106(46):19563–19568

Clark DJ, Ting LH, Zajac FE, et al (2010) Merging of healthy motor modules predicts reduced locomotor performance and muscle coordination complexity post-stroke. *Journal of neurophysiology* 103(2):844–857

D'agostino RB, Belanger A, D'Agostino Jr RB (1990) A suggestion for using powerful and informative tests of normality. *The American Statistician* 44(4):316–321

Danion F, Galléa C (2004) The relation between force magnitude, force steadiness, and muscle co-contraction in the thumb during precision grip. *Neuroscience letters* 368(2):176–180

d'Avella A, Saltiel P, Bizzi E (2003) Combinations of muscle synergies in the construction of a natural motor behavior. *Nature neuroscience* 6(3):300–308

Ferrante L, Boesendorfer A, Barsakcioglu DY, et al (2025) Implanted microelectrode arrays in reinnervated muscles allow separation of neural drives from transferred polyfunctional nerves. *Nature Biomedical Engineering* pp 1–16

Festin C, Ortmayr J, Maierhofer U, et al (2024) Creation of a biological sensorimotor interface for bionic reconstruction. *Nature Communications* 15(1):5337

Franklin DW, Osu R, Burdet E, et al (2003) Adaptation to stable and unstable dynamics achieved by combined impedance control and inverse dynamics model. *Journal of neurophysiology*

Holobar A, Zazula D (2007) Multichannel blind source separation using convolution kernel compensation. *IEEE Transactions on Signal Processing* 55(9):4487–4496

Holobar A, Minetto MA, Botter A, et al (2010) Experimental analysis of accuracy in the identification of motor unit spike trains from high-density surface emg. *IEEE Transactions on Neural Systems and Rehabilitation Engineering* 18(3):221–229

Holobar A, Minetto MA, Farina D (2014) Accurate identification of motor unit discharge patterns from high-density surface emg and validation with a novel signal-based performance metric. *Journal of neural engineering* 11(1):016008

Huang S, Huang H (2018) Voluntary control of residual antagonistic muscles in transtibial amputees: reciprocal activation, coactivation, and implications for direct neural control of powered lower limb prostheses. *IEEE Transactions on Neural Systems and Rehabilitation Engineering* 27(1):85–95

Kuiken TA, Dumanian GA, Lipschutz RD, et al (2004) The use of targeted muscle reinnervation for improved myoelectric prosthesis control in a bilateral shoulder disarticulation amputee. *Prosthetics and orthotics international* 28(3):245–253

Kung TA, Langhals NB, Martin DC, et al (2014) Regenerative peripheral nerve interface viability and signal transduction with an implanted electrode. *Plastic and reconstructive surgery* 133(6):1380–1394

Lee D, Seung HS (2000) Algorithms for non-negative matrix factorization. *Advances in neural information processing systems* 13

McGill KC, Lateva ZC, Marateb HR (2005) Emglab: an interactive emg decomposition program. *Journal of neuroscience methods* 149(2):121–133

Muceli S, Boye AT, d'Avella A, et al (2010) Identifying representative synergy matrices for describing muscular activation patterns during multidirectional reaching in the horizontal plane. *Journal of neurophysiology* 103(3):1532–1542

Muceli S, Poppendieck W, Holobar A, et al (2022) Blind identification of the spinal cord output in humans with high-density electrode arrays implanted in muscles. *Science advances* 8(46):eab05040

Pettersen E, Sassu P, Pedrini FA, et al (2024) Targeted muscle reinnervation: Surgical protocol for a randomized controlled trial in postamputation pain. *Journal of Visualized Experiments* 2024(205):e66379

Pierrot-Deseilligny E, Burke D (2005) The circuitry of the human spinal cord: its role in motor control and movement disorders. Cambridge university press

Poscente SV, Peters RM, Cashaback JG, et al (2021) Rapid feedback responses parallel the urgency of voluntary reaching movements. *Neuroscience* 475:163–184

Proske U, Gandevia SC (2012) The proprioceptive senses: their roles in signaling body shape, body position and movement, and muscle force. *Physiological reviews*

Seyedali M, Czerniecki JM, Morgenroth DC, et al (2012) Co-contraction patterns of trans-tibial amputee ankle and knee musculature during gait. *Journal of neuroengineering and rehabilitation* 9(1):29

Wood SJ, Slater CR (2001) Safety factor at the neuromuscular junction. *Progress in neurobiology* 64(4):393–429

Zuniga JM, Dimitrios K, Peck JL, et al (2018) Coactivation index of children with congenital upper limb reduction deficiencies before and after using a wrist-driven 3d printed partial hand prosthesis. *Journal of neuroengineering and rehabilitation* 15(1):48